Acta Oceanologica Sinica 2006, Vol. 25, No. 5, p. 1 ~ 13
http://www.oceanpress.com.cn
E-mail: hyxbe@263.net

Meso-scale available gravitational potential energy in the world oceans

FENG Yang[1], WANG Wei[1*], HUANG Ruixin[2]

1. Physical Oceanography Laboraltory, Ocean University of China, Qingdao 266003, China
2. Department of Physical Oceanography, Woods Hole Oceanographic Institution, Woods Hole, MA 02543, USA

Received 2 November 2005, accepted 29 April 2006

Abstract

The pitfalls of applying the commonly used definition of available gravitational potential energy (AGPE) to the world oceans are re-examined. It is proposed that such definition should apply to the meso-scale problems in the oceans, not the global scale. Based on WOA98 climatological data, the meso-scale AGPE in the world oceans is estimated. Unlike previous results by Oort et al., the meso-scale AGPE is large wherever there is a strong horizontal density gradient. The distribution of meso-scale AGPE reveals the close connection between the baroclinic instability and the release of gravitational potential energy stored within the scale of Rossby deformation radius.

Key words: energy of ocean circulation, available potential gravitational energy, meso-scale, baroclinic instability, Rossby deformation radius

1 Introduction

The oceanic general circulation takes place in the environments of gravity. As a mechanical system, the oceanic circulation requires sources of mechanical energy to overcome friction and dissipation. Although the ocean receives a huge amount of thermal energy from solar radiation and the atmosphere, it cannot convert the thermal energy efficiently. In fact, the oceanic circulation is not a thermal engine; instead, it is a conveyer driven by external sources of mechanical energy from wind and tides. Therefore, the mechanical energy, in particular, the balance of gravitational potential energy (GPE) plays a vital role in the energetics of the oceanic circulation (Huang, 2004). Using the mean depth of the world ocean, $z = 3750$ m, and the reference level, the total amount of GPE in the world oceans is estimated at 20.9 YJ (Oort et al., 1994). However, most part of such huge amount of energy is dynamically inert, and only a very small fraction, the available gravitational potential energy (AGPE), is dynamically active.

The concept of AGPE was first introduced by Margules (1905). However, the application of this concept to the dynamics of atmosphere appeared primarily after Lorenz (1955) introduced an approximate definition for AGPE. Different forms of AGPE

* Corresponding author, E-mail: wei@ouc.edu.cn

have been proposed for the study of the ocean. For an incompressible ocean, AGPE is defined as

$$\chi = g\int(z - Z)\mathrm{d}m, \qquad (1)$$

where g is the gravitational acceleration; z and Z are the geopotential height of a mass element in the physical and reference states.

The reference state is defined as a state with minimal GPE. For the case of an incompressible ocean such a reference state can be found through a single sorting (Huang, 1998). Owing to the nonlinear equation of state of the seawater, searching such a state of minimal GPE in the ocean is complicated. In previous studies the horizontal mean density profile has been used as the reference state as a compromise. For example, Wright (1972) discussed the deep circulation of Atlantic, using such a reference state to infer the rate of the release of AGPE in the Atlantic. In many previous studies for the oceanic circulation AGPE is calculated according to the following definition (Oort et al., 1989; Oort et al., 1994; Reid et al., 1981):

$$\prod^{a} = -g\iiint\frac{(\rho - \bar{\rho}(z))^2}{\bar{\rho}_z^{\theta}}\mathrm{d}x\mathrm{d}y\mathrm{d}z, \qquad (2)$$

where the reference state $\bar{\rho}(z)$ is defined by horizontally averaging the density field; and $\bar{\rho}_z^{\theta}$ is the vertical gradient of the horizontal-mean potential density.

Since this definition is equivalent to that used in quasi-geostrophic dynamics (Pedlosky, 1987), it has been called the quasi-geostrophic AGPE (QG AGPE hereafter) (Huang, 1998; 2005). Note that in this study the vertical gradient of potential density was calculated as follows: first, the potential density at levels ($k+1$) and ($k-1$) was calculated, using the Pressure at Level k as the reference pressure; second, a central difference was used to calculate the vertical gradient of potential density at Level k.

Although this definition is simple and easy to use, it has some problems as well. First, although quasi-geostrophy is a sound approximation for the study of meso-scale eddies and baroclinic instability, it is inaccurate for the study of thermohaline circulation. It is found that the application of this traditional definition of AGPE and its sources can lead to substantial errors, as shown in the case of an incompressible ocean by Huang (1998). Second, the contribution due to internal energy is not clearly defined in this formulation. Thirdly, as discussed by Huang (2005), horizontal mixing of density field is required during the adjustment from the physical state to the reference state; thus, this definition is not based on truly adiabatic processes. Furthermore, a close examination reveals that such a horizontal shifting of water mass does not change the total GPE; thus, the meaning of AGPE defined in this way remains unclear.

Despite of the problems existed in the QG AGPE for application to the study of basin-scale dynamics; there is no question that such a definition remains a very powerful tool in the study of meso-scale dynamics, in particular in understanding the baroclinic instability. It is well-known that GPE of the mean state is released and converted into kinetic energy and potential energy of meso-scale eddies. Therefore, it is important to explore whether we can find a suitable way to use this commonly accepted definition of AGPE. As will be discussed shortly, the best way is to limit its use for problems with horizontal scale on the order of deformation radius. Accordingly, we will call such a definition meso-scale AGPE (MS AGPE hereafter). On the other hand, for dynamical processes associated with basin-scale, the exact definition of AGPE should apply, as discussed by Huang (2005).

In this study we will be focused on the MS AGPE in the world oceans. First, we derive a formula appropriate for meso-scale phenomena in Section 2. Combining with climatological grid data, we apply this formula to the distribution of MS AGPE in

the world oceans in Section 3. This study is concluded in Section 4.

2 Formula and method for calculation

Our calculation was based on WOA98(Levitus et al. , 1998) climatology data, with a horizontal resolution of 1° × 1° and 33 levels in the vertical direction. Here the UNESCO equation of state (Fofonoff and Millard 1983) was used in the density and potential density calculation. For comparison, we carried out four calculations in which the same formula (2) was used.

Case A: Eq. (2) was applied to a global 1° × 1° grids, i. e. , the density obtained by horizontally averaging over the 1° × 1° grid cell was used as $\bar{\rho}$ in Eq. (2); results from this calculation will be referred to as MS1 AGPE hereafter. The corresponding finite difference scheme (see Appendix A) is:

$$\prod_{i,j}^{a} = -\frac{g}{24}\sum_{k=1}^{km}\left(\rho_x^2 + \rho_y^2 + \frac{1}{12}\rho_\Delta^2\right)(\bar{\rho}_z^{\theta})^{-1}A\Delta Z_k. \quad (3)$$

Case B: Eq. (2) was applied to a global 2° × 2° grid, and the results will be referred to as MS2 AGPE. In this case, the density horizontally averaged over the 2° × 2° grid cell was used as the reference density $\bar{\rho}$. Equation (2) is reduced to the following finite deference form (see Appendix):

$$\prod_{i,j}^{a} = -\frac{g}{2}\sum_{k=1}^{km}\sum_{i=1}^{4}\left[\frac{1}{12}\left(\rho_{x,j}^2 + \rho_{y,i}^2 + \frac{1}{12}\rho_{\Delta,i}^2\right) + (\bar{\rho}_i - \bar{\bar{\rho}})^2\right](\bar{\bar{\rho}}_z^{\theta})^{-1}A_i\Delta Z_k \quad (4)$$

where $\bar{\rho}_i$ is the average density in one of each four sub-cells in the 2° × 2° grid cell; the reference state density $\bar{\bar{\rho}}$ is the horizontal average density of those four sub-cells; $\bar{\bar{\rho}}_z^{\theta}$ is the average vertical gradient of potential density in this cell; and A_i represents the area of a sub-cell. For the meaning of $\rho_{x,i}$, $\rho_{y,i}$, $\rho_{\Delta,i}$ and the derivation, the reader may refer to the Appendix A.

Case C: Eq. (2) was applied to the individual basins in the world oceans, and the results will be referred to as BA AGPE hereafter. Therefore, the horizontal-mean density and the vertical gradient of potential density in each basin were used in Eq. (2) accordingly.

Case D: Eq. (2) is applied to the world oceans, and the results will be referred to as GL AGPE hereafter. In this calculation, the density profile obtained by horizontally averaging over the global oceans was used as $\bar{\rho}(z)$, and the corresponding global mean vertical potential density gradient was used as $\bar{\rho}_z^{\theta}$. Note that the result obtained from this case is parallel to that obtained by Oort et al. (1994), and any difference between our results presented here and Oort et al. (1994) is due to the data quality (Oort et al. used an old data set with a very low resolution of 4° × 5°) and the finite difference schemes are used in the calculation.

Note that for Cases A and B some inland seas and semi-closed basins were excluded from our calculation, such as the Mediterranean Sea, Red Sea, and Hadson Sea. Besides, in the Northern Hemisphere our calculation was limited to 70° N; thus, the Arctic Ocean was excluded.

3 Results and analysis

3.1 Global sum of AGPE

The total amount of AGPE and its horizontal distribution calculated from these cases are different. First of all, the total amount of AGPE increases dramatically, as the horizontal scale used to calculate the reference density $\bar{\rho}$ increases (see Table 1). Note that for Case C, the calculation was carried out for 14 basins, and the corresponding results are listed in Table 2. The large difference in the total amount of AGPE calculated in these four cases can be easily explained through the definition of Eq. (2). Assuming the density is a linear function in space,

AGPE calculated from Eq. (2) is linearly proportional to the square of the grid size. Therefore, as the horizontal scale of density averaging increases from 1° to 2°, to the basin scale, and eventually the global scale, the total amount of AGPE increases 1 000 times (Table 1).

Table 1. Global sum of AGPE(EJ) of all cases. Values in the last column are the total amount of AGPE and the net AGPE, calculated from the exact definition of AGPE, as discussed by Huang (2005)

	Case				Exact
	A(MS1)	B(MS2)	C(BA)	D(GL)	
AGPE/EJ	1.07	8.22	344	1277	1880(811)

Table 2. BA AGPE (EJ) in different basins

Basin	BA AGPE/EJ	Basin	BA AGPE/EJ
North Pacific	21.6	Arctic Ocean	51.0
North Atlantic	15.2	Gulf of Mexico	0.296
North Indian	1.58	South China Sea	0.754
South Pacific	19.7	Indonesia seas	1.65
South Atlantic	6.13	Mediterranean	0.26
South Indian	15.0	Sea of Japan	0.51
Southern Ocean	210	Hadson Bay	0.005
Sum	344		

Which calculation gives the best estimate of global sum of AGPE? MS1 AGPE gives a global sum of 1.07 EJ, which is 9/10 smaller than the total amount of meso-scale energy in the world oceans, 13 EJ estimated by Zang and Wunsch (2001). Since meso-scale eddies obtain their energy primarily from AGPE, this estimated amount of AGPE (1.07 EJ) may not be large enough to support the meso-scale activity, and, thus, the total amount of AGPE calculated from MS1 AGPE seems to be too small.

By doubling the grid size, the global integrated MS2 AGPE is 8.22 EJ, which is comparable to the total kinetic energy of meso-scale eddies, 13 EJ. Choosing such a 2° × 2° grid can be linked to the preferred horizontal scale for the baroclinic instability. The major density fronts in the world oceans are mostly located at middle latitudes, where the first baroclinic radius of deformation is about 40 km. The typical wave length of meso-scale eddy is estimated at 2π times the Rossby deformation radius, and this corresponds to approximately 200 km at middle latitudes; thus, a 2° × 2° grid is the optimal size to catch the GPE available through the baroclinic instability. At higher latitudes, the first deformation radius is reduced to 20 km or less, but the zonal length of our 2° grid is also reduced to the order of 120 km; thus, it seems a suitable choice. Note that at low latitudes, the deformation radius is on the order of 200 km or more, so our 2° grid may not be a good choice for the meso-scale phenomena there. However, our 2° × 2° grid seems a good compromise for the world oceans.

Note that the reference state used in this calculation is a density field which is piecewise constant within the 2° × 2° grid cell. It is clear that such a reference state is not a state of minimal gravitation

potential energy for the world oceans because the additional adjustment of the density field is possible to low down the GPE further. Therefore, the total MS AGPE calculated in this way is much smaller than the total amount of GPE that can be released from the initial state; instead, the horizontal distribution of MS2 AGPE provides us important information regarding the potential energy source supporting the baroclinic instability on the scale of deformation radius.

On the other hand, both the BA and GL AGPE give a much large amount of global sum of AGPE (see Table 1). Incidentally, the total amount of AGPE calculated from the GL definition fells between the AGPE and APE calculated from the exact definition of AGPE discussed by Huang (2005). However, applying these two definitions to the world oceans is theoretically inappropriate. As discussed by Huang (1998, 2005) and summed up in the introduction, such applications violate the fundamental assumptions, such as the adiabatic adjustment from the physical state to the reference state. The pitfalls of these two definitions will be further illustrated through analysis of the results obtained in the following discussion.

The most remarkable contrast is between MS1 AGPE and GL AGPE, which reflects the essential differences between the potential adjustment processes implied in these two definitions. In the following discussion a detailed description of MS1 AGPE distribution will be presented and compared with that obtained from Case D, i. e. , the GL AGPE.

3.2 Global distribution of AGPE

MS1 AGPE distribution in the world oceans calculated from Eq. (3) shows a very interesting picture (see Fig. 1). The most remarkable feature is the high-density of MS1 AGPE associated with strong density fronts, including the western boundary currents, such as the Kuroshio and Gulf Stream between 20° and 40°N (with a MS AGPE density of 2 KJ/m^2), and Antarctic Circumpolar Current (ACC hereafter; with a MS AGPE density of 9 KJ/m^2). The total MS AGPE stored in the Southern Ocean is approximately 0. 8EJ, which is almost three times larger than the Northern Hemisphere. Distribution of AGPE calculated from Case B has a feature very similar to that from Case A, except for slightly more diffusive features due to a lower spatial resolution.

In comparison, the distribution of GL AGPE calculated using a reference state defined as the global horizontal-mean density, is quite different from two MS AGPE. Note that the units used in Fig. 2 is 1 000 times larger than that in Fig. 1 because the scale used to calculated the horizontal mean density in this case is much larger than in Fig. 1; the reason for such a huge difference in magnitude has been discussed above. It is readily seen that high GL AGPE values primarily appear in the western equatorial Pacific and at high latitudes, such as around 60°S in the Southern Hemisphere and in the Greenland – Norwegian Sea in the Northern Hemisphere (see Fig. 2). Note that although ACC is a high-value area of AGPE in both GL AGPE and MS AGPE, there is a big difference in the exact location. In the case of GL AGPE, the maximum appears around the southern edge of ACC, at the latitude band of 60°S; while the high-value areas of MS AGPE appear at the latitude of 50°S and near the core of the fronts in ACC.

The difference in the distribution of AGPE between these two cases reflects the essential difference in the fundamental assumptions made in these two definitions. In the case of GL AGPE, the strength of AGPE at a given location is assumed to be proportional to the difference in the local density and the global horizontal-mean density. Since the surface density in the ocean interior at middle latitudes is close to the global horizontal mean, GL AGPE is small in such areas. On the other hand, the density

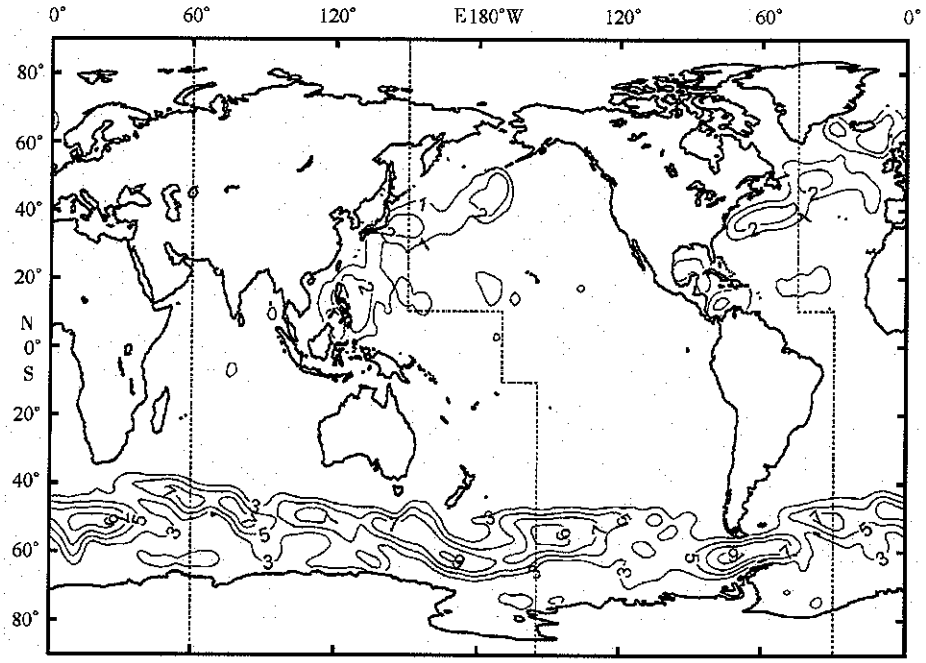

Fig. 1. Horizontal distribution of the vertically integrated MS1 AGPE (KJ/m^2) in the world oceans.

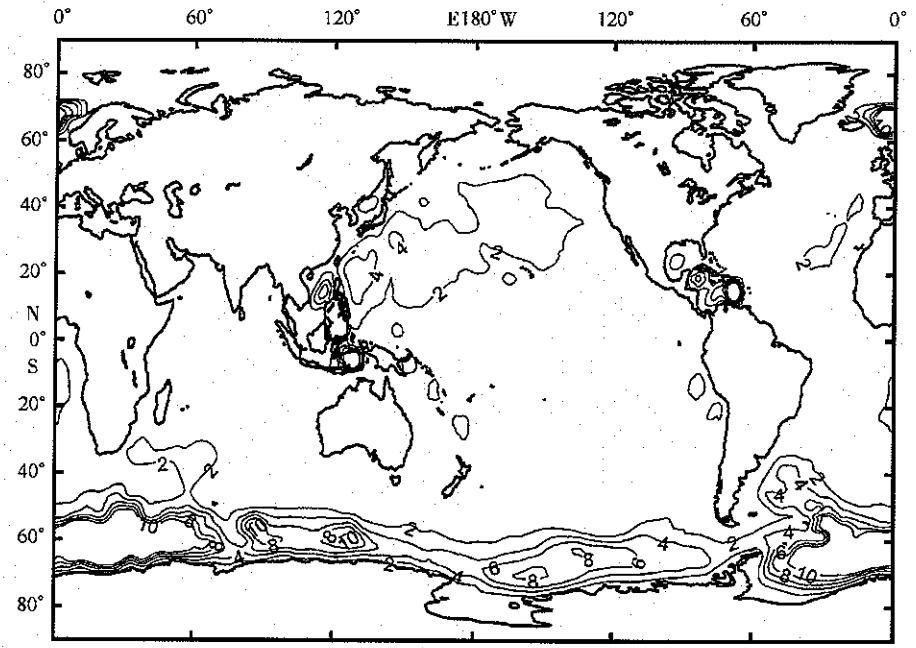

Fig. 2. Horizontal distribution of the vertically integrated GL AGPE. (MJ/m^2) in the world oceans.

in the western equatorial Pacific is much smaller than the global mean, and the density at high latitudes is much larger than the global horizontal mean. As a result, GL AGPE shows high value in both high latitudes and Western Equatorial Pacific (Fig. 2). These areas with a high value of GL AGPE are the artifacts of applying AGPE applied to the global scale, and they are not related to realistic physical processes in the world oceans (Huang, 1998, 2005). On the other hand, areas of high MS AGPE

are closely linked to the baroclinic instability associated with strong density fronts in the world oceans, and they are the most interesting sites for the study of meso-scale dynamics.

The close link between the major density fronts and MS AGPE in the world oceans can be seen clearly on horizontal maps of MS AGPE distribution at constant depths; as an example, a map for the MS1 AGPE density at the 200 m depth is shown in Fig 3. The high-value areas include the core of ACC with density higher than 1.8 J/m^3, the Kuroshio and its extension with density higher than 1.6 J/m^3, the Gulf Stream and the North Atlantic Current with density higher than 1.6 J/m^3, the North Equatorial Current with density higher than 0.8 J/m^3, and the major currents associated with the subtropical gyres in the South Pacific and South Indian Oceans. These outstanding features do not appear in the corresponding horizontal map of GL AGPE (figure not included).

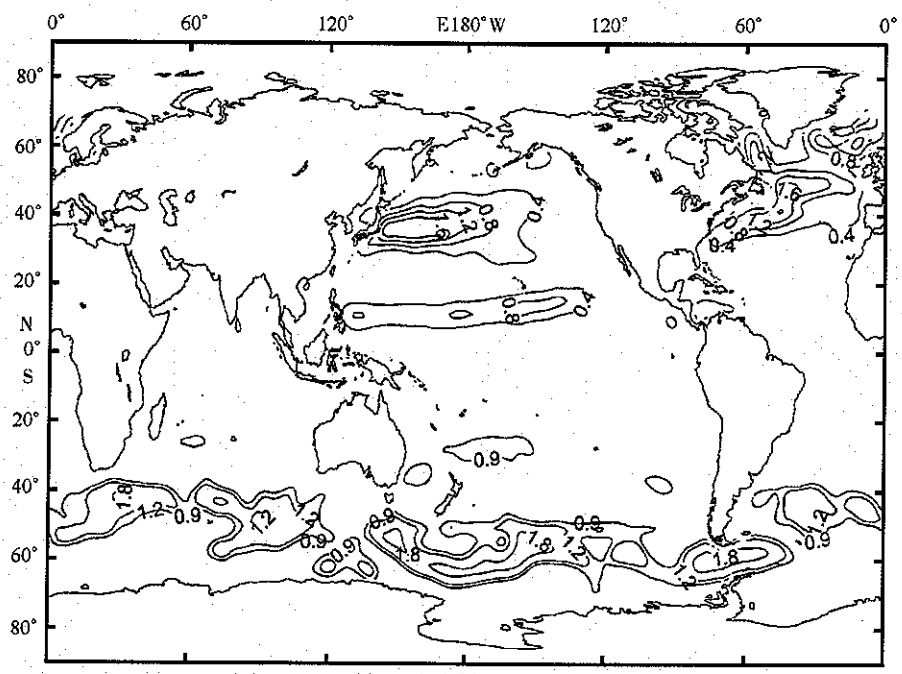

Fig. 3. Horizontal distribution of MS1 AGPE (J/m^3) at the depth of 200 m.

3.3 Meridional distribution of AGPE

To clearly show the structure associated with density fronts in a single map and avoid the land mass, the following composite meridional distribution of MS1 AGPE is presented here: it combines a section from 75°S to 10°N at 30°W and a section from 10° to 60°N along 45°W (see Figs 4 and 5, dash lines in Fig. 1 depict positions of these sections). The cores of ACC appear as a local maximum at the latitude of 50°S and at the depth of 300 ~ 1 500 m, with a value higher than 3 J/m^3. The Gulf Stream appears as a maximum at the latitude of 40°N and in the upper 500 m.

On a close examination, all major currents and frontal structures in the upper ocean through this section can be clearly identified from a map for the upper ocean (see Fig. 5). At least four outstanding frontal structures can be clearly identified in the upper 100 m. The equatorial current system can be unmistakably linked to the frontal structure in the upper 500 m.

For comparison, the meridional distribution of GL AGPE along the same meridional section looks quite different. In contrast to the distribution of MS1 AGPE, the high-value contours appearing in the GL AGPE section map (Fig. 6) are mostly confined to high latitudes, such as south of 60°S in the Southern Hemisphere and north of 50°N; these high-value areas are not related to strong fronts in the oceans and any other potential physical processes in the oceans. As such, these features are artifacts of the GL AGPE definition, and they should be treated with caution (Huang, 1998, 2005).

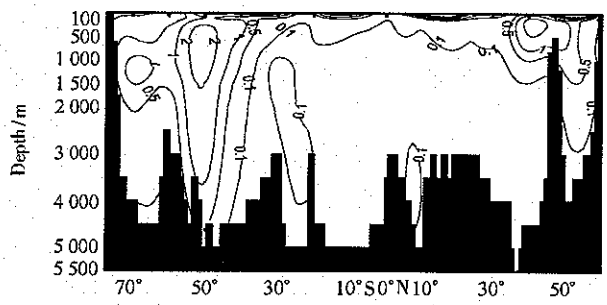

Fig. 4. A composite (see the text) meridional section of MS1 AGPE density (J/m^3) distribution in the Atlantic.

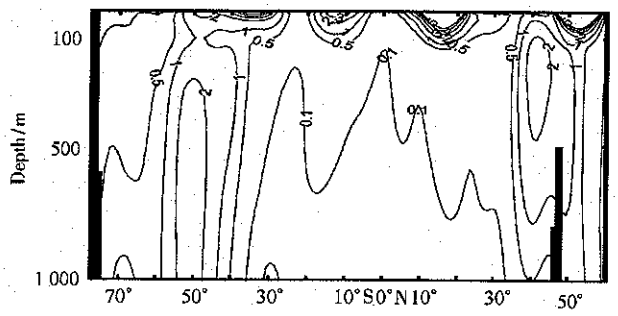

Fig. 5. The corresponding MS1 AGPE density (J/m^3) distribution in the upper ocean.

A composite meridional distribution of MS1 AGPE in the Pacific Ocean is shown in Figs 7 and 8. These maps are composite of three segments: a segment along 150°E from 10° to 60°N, a segment along 170°W from 10°S to 10°N, and another segment along 155°W from 10° to 75°S. All the major zonal currents in the Pacific appear as remarkable

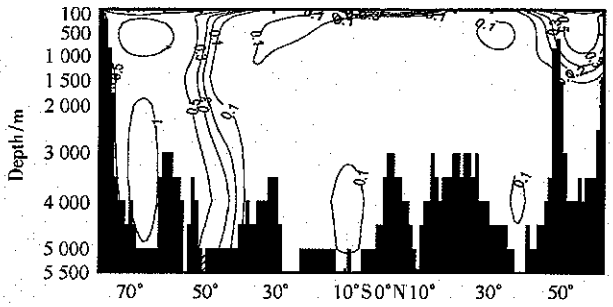

Fig. 6. The corresponding meridional section of GL AGPE density (×10 kJ/m^3) distribution in the Atlantic.

features in these two maps. Similar to the situation in the Atlantic Ocean, contours with maximal values appear in the latitudinal band of 40° ~ 60°S, with the maximal value exceeding 5 J/m^3 and extending from the surface to the depth of 700 m. In the Northern Hemisphere, high value of MS1 AGPE appears as three cores in the upper ocean: a surface trapped maximum at 5°N, corresponding to the westward North Equatorial Countercurrent; a subsurface maximum at 20°N, corresponding to the North Equatorial Current; and a third outstanding maximum at 38°N, corresponding to the strong east-moving Kuroshio. The core of Kuroshio extends all the way to the depth of 1 000 m at this section (see Fig. 8).

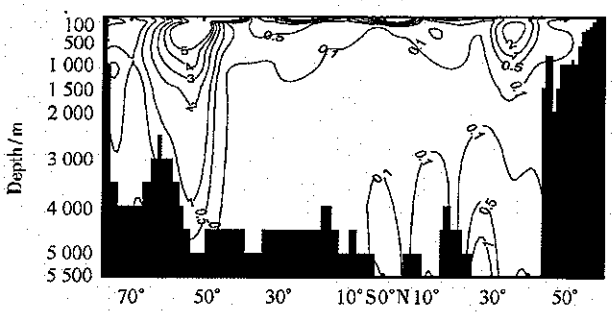

Fig. 7. A composite meridional section (see text) of MS1 AGPE density (J/m^3) distribution in the Pacific.

The corresponding meridional distribution of GL AGPE is shown in Fig. 9. Similar to the corresponding meridional map in the Atlantic, high-value GL AGPE contours are confined to high latitudes and equatorial band, with no specific link with the strong

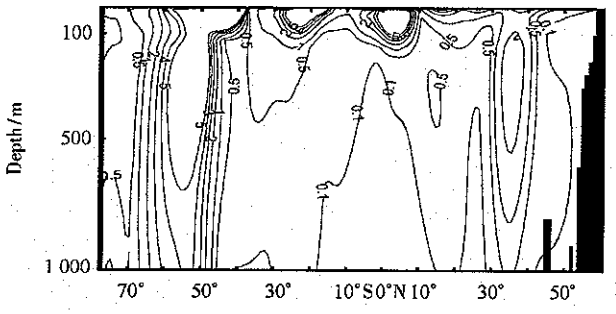

Fig. 8. The corresponding MS1 AGPE density (J/m^3) distribution in the upper ocean.

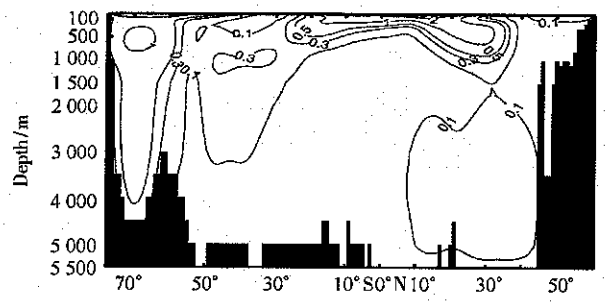

Fig. 9. The corresponding meridional section of GL AGPE density ($\times 10$ kJ/m^3) distribution in the Pacific.

currents in the oceans.

The distribution of MS1 AGPE along 60° E in the Indian Ocean is shown in Fig. 10. Similar to the previous two sections in the Atlantic and the Pacific, here again the high-value contours of MS1 AGPE are located around 50°S, apparently the same location of the core of ACC, with a maximal value of 5 J/m^3 in the core of ACC. The corresponding distribution of GL AGPE along this section is shown in Fig. 11. Although there are local maxima in the Southern Hemisphere, their location is either north of the core of ACC or south of the core, i. e. , at the high latitudinal edge of ACC.

3.4 Zonally integrated distribution of MS AGPE and GL AGPE

Finally, we present the zonally integrated distribution of AGPE (Fig. 12). Note that in order to show the noticeable distinction among them, they

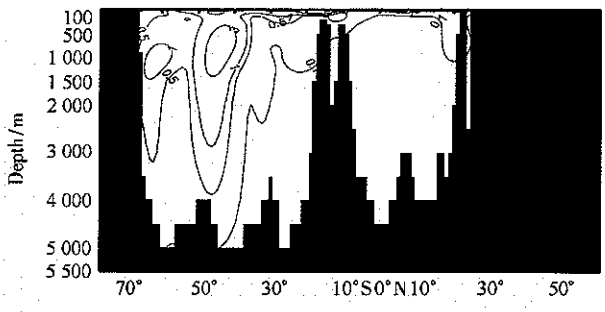

Fig. 10. A meridional section along 60°E of the MS1 AGPE density (J/m^3) distribution in the Indian Ocean.

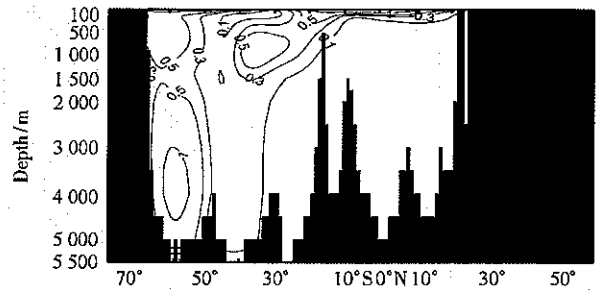

Fig. 11. The corresponding meridional section along 60°E of the GL AGPE density ($\times 10$ kJ/m^3) distribution in the Indian Ocean.

were drawn on the same panel with different units; thus, the scale of GL AGPE is 10 times larger than MS2 AGPE, and MS2 AGPE is 10 times larger than MS1 AGPE.

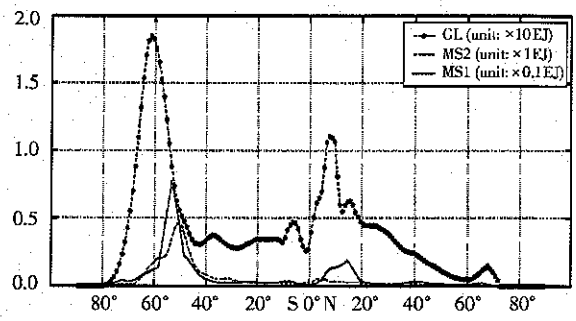

Fig. 12. There AGPE integral values distribution along each 1° latitude band; note different units used for each case.

The major difference between these three cases is summarized in this figure. Here again, the high

value of GL AGPE appears at low latitudes (0° ~ 20° N), with a total value of more than 10 EJ, and at latitudes higher than 60°S, with a total value of more than 15 EJ. The existence of these high-value areas is due to the large departure of location density to the global mean. In contrast, the high-value area of MS AGPE exists between 40° and 60°S, with a total value approximate to 0.5 EJ for MS2 and above 0.05 EJ for MS1. In the case of MS AGPE, the core of ACC stands as the most important site of high value area in the world oceans, and this is consistent with the physical processes associated with the strong multiple fronts associated with ACC, where GPE is continuously being released through baroclinic instability. In addition, MS1 AGPE is large north of the equator for the same reason.

4 Conclusions

Since application of the traditional definition of AGPE to the world oceans is questionable, we re-examined the definition of AGPE. Based on the dynamical framework of meso-scale dynamics and baroclinic instability, we argued that the same formula is applicable to the meso-scale problem, not the global-scale problem. In contrast to the previous studies by Oort et al. (1994), where the same formula was used to calculate the AGPE, i. e. , using the basin-mean density as the reference density, we demonstrated that using the same formula to meso-scale problems, i. e. , using the density averages over a meso-scale grid as the reference density, can produce a very informative map of AGPE distribution in the world oceans, which is closely linked to the strong density fronts and currents in the oceans. On the other hand, our calculation demonstrated that the application of GL AGPE can lead to maps of AGPE which is unphysical.

Note that MS AGPE distribution is closely related to the baroclinic instability in the oceans. In fact, the MS AGPE definition is directly linked to the rate of GPE transformation from the mean state to eddies, which is commonly parameterized in terms of the Gent-McWilliam scheme (Gent et al. , 1995) and other variations of the scheme. The major uncertainty involved in such a scheme is the so-called eddy diffusivity. Assuming certain formulae for the eddy diffusivity, which may not necessarily be constant in time or space, the MS AGPE discussed here is immediately linked to the conversion from the mean state GPE to the eddies. For the transform of energy from the mean state to the eddies in the world oceans, the reader may refer to Huang and Wang (2003); however, the exact nature of this connection is a matter of hot debate, and it is thus beyond the scope of this study.

In addition to the recent work by Huang (1998, 2005), thus, we postulate that there are two distinctly different definitions of AGPE, and they can be used as diagnostic tools in the study of oceanic circulation. First, there is a MS AGPE discussed in this study, which can be used to diagnose the AGPE associated with the strong density fronts and currents in the system. MS AGPE is available for the meso-scale activity, such as the baroclinic instability; thus, it is useful for the study of meso-scale activity in the circulation system.

Second, there is the exact definition of AGPE, as discussed by Huang (1998, 2005). The exact definition of AGPE can be used as a powerful tool in diagnosing the energetics of the basin-scale circulation, i. e. , the mean current of basin-scale. For example, the energetics of the basin-scale circulation over the decadal time scale or the centennial time scale can be examined, using the exact definition of AGPE.

Note that these two definitions may provide information about the oceanic circulation on different horizontal scales and temporal scales, which are compensating each other; thus, they may be used at

the same time to diagnose the structure and time evolution of the system. The application of both definitions to the same circulation problem will provide existing information about the system, and a test study is currently under way.

Acknowledgements

Feng Yang and Wang Wei were supported by the National Naturale Science Foundation of China under contract No. 40476010 and the Research Fund for the Doctoral Program of Higher Education of China under contract No. 20030423011, Huang Ruixin was supported by the Van Alan Clark Chair of the Woods Hole Oceanographic Institution, Woods Hole Contribution under contract No. 11209.

References

Fofonoff N P, Millard R C. 1983. Algorithms for computation of fundamental properties of seawater. UNESCO Technical Papers in Marine Science 44, 53

Gent P R, Willebrand J, McDougall T J, et al. 1995. Parameterizing eddy-induced tracer transports in ocean circulation models. J Phys Oceanogr, 25: 463 ~ 474

Huang Ruixin. 1998. Mixing and available potential energy in a Boussinesq ocean. J Phys Oceanogr, 28: 669 ~ 678

Huang Ruixin. 2004. Ocean, energy flows. In: Cleveland C J, ed. Encyclopedia of Energy, v4. Elsevier, 497 ~ 509

Huang Ruixin. 2005. Available potential energy in the worlds oceans. J Mar Res, 63: 141 ~ 158

Huang Ruixin, Wang Wei. 2003. Gravitational potential energy sinks in the oceans. Near-boundary Processes and Their Parameterization, Proceedings. Hawaii Winter Workshop, 239 ~ 247

Levitus S, Boyer T, Conkright M E, et al. 1998. World Ocean Database 1998: v1. Introduction, NOAA Atlas NESDIS 18. Natl Oceanic and Atmos Admin, US Dep of Commer, Washington D C, 346

Lorenz E N. 1955. Available potential energy and the maintenance of the general circulation. Tellus, 7: 157 ~ 167

Margules M. 1905. Uber die energie der sturme. Wein: K. K. Hof-und. Stattsdruckerei, 26

Oort A H, Ascher S C, Levitus S, et al. 1989. New estimates of the available potential energy in the world ocean. J Geophy Res, 94: 3 187 ~ 3 200

Oort A H, Anderson L A, Peixoto J P. 1994. Estimates of the energy cycle of the oceans. J Geophy Res, 99:7 665 ~ 7 688

Pedlosky J. 1987. Geophysical Fluid Dynamics. New York: Springer-Verlag, 710

Reid R O, Elliott B A, Olson D B. 1981. Available potential energy: a clarification. J Phys Oceanogr, 11:15 ~ 29

Wright W R. 1972. Northern sources of energy for the deep Atlantic. Deep-Sea Res, 19(12): 865 ~ 877

Zang X, Wunsch C. 2001. Spectral description of low frequency oceanic variability. J Phys Oceanogr, 31: 3 073 ~ 3 095

Appendix A
Available gravitational potential energy for 1° × 1° and 2° × 2° grid cells

1 Formula for the 1° × 1° grid cell

Assuming the grid cell in question is within the four grids (i,j), $(i+1,j)$, $(i,j+1)$, and $(i+1,j+1)$. It is more convenient to use the center of the grid cell as the origin of the new local Cartesian coordinates (x,y). Assuming the density distribution within this grid cell is a bi-linear function of the local coordinates, we have the following expression of density distribution within this grid cell:

$$\rho = \rho_x x + \rho_y y + \rho_\Delta xy + \bar{\rho},$$

$$\rho_x = \frac{1}{2}(\rho_{i+1,j} + \rho_{i+1,j+1}) - \frac{1}{2}(\rho_{i,j} + \rho_{i,j+1}),$$

$$\rho_y = \frac{1}{2}(\rho_{i,j+1} + \rho_{i+1,j+1}) - \frac{1}{2}(\rho_{i,j} + \rho_{i+1,j}),$$

$$\rho_\Delta = (\rho_{i,j} + \rho_{i+1,j+1}) - (\rho_{i,j+1} + \rho_{i+1,j}),$$

$$\bar{\rho} = \frac{1}{4}(\rho_{i,j} + \rho_{i,j+1} + \rho_{i+1,j} + \rho_{i+1,j+1}).$$

Thus, simple integration reduces Eq.(2) to the following finite difference form:

$$\prod_{i,j}^{a} = -\frac{g}{24}\sum_{k=1}^{km}\left(\rho_x^2 + \rho_y^2 + \frac{1}{12}\rho_\Delta^2\right)(\bar{\rho}_z^\theta)^{-1}A\Delta Z_k,$$

where km is the lowest level of the water column in the grid cell; $\bar{\rho}_z^\theta$ is the horizontal-mean vertical gradient of potential density within this grid cell; and A is the area of the grid cell.

2 Formula for the 2° × 2° grid cell

As Fig. A1 shows, there are nine points and four sub-cells in a 2° × 2° grid cell. The densities of these points are $\rho_{i-1,j-1}, \rho_{i-1,j}, \rho_{i-1,j+1}, \rho_{i,j-1}, \rho_{i,j}, \rho_{i,j+1}, \rho_{i+1,j-1}, \rho_{i+1,j}, \rho_{i+1,j+1}$, respectively, and areas of the sub-cells are A_1, A_2, A_3, A_4. Assume density in each sub-cell is a bi-linear function in the local Cartesian coordinates (x, y), with the origin at the center of each grid sub-cell. For example, the density within the first sub-cell is in forms:

$$\rho = \rho_{x,1} x + \rho_{y,1} y + \rho_{\Delta,1} xy + \bar{\rho}_1,$$

$$\rho_{x,1} = \frac{1}{2}(\rho_{i-1,j+1} + \rho_{i,j+1}) - \frac{1}{2}(\rho_{i-1,j} + \rho_{i,j}),$$

$$\rho_{y,1} = \frac{1}{2}(\rho_{i-1,j} + \rho_{i-1,j+1}) - \frac{1}{2}(\rho_{i,j+1} + \rho_{i,j}),$$

$$\rho_{\Delta,1} = (\rho_{i,j} + \rho_{i-1,j+1}) - (\rho_{i,j+1} + \rho_{i-1,j}),$$

$$\bar{\rho}_1 = \frac{1}{4}(\rho_{i-1,j} + \rho_{i-1,j+1} + \rho_{i,j+1} + \rho_{i,j}).$$

Similarly, the density distribution in other sub-cells can be derived accordingly, with the following notations: $\rho_{x,2}, \rho_{y,2}, \rho_{\Delta,2}, \bar{\rho}_2, \rho_{x,3}, \rho_{y,3}, \rho_{\Delta,3}, \bar{\rho}_3, \rho_{x,4}, \rho_{y,4}, \rho_{\Delta,4}, \bar{\rho}_4$. The average density of this $2° \times 2°$ grid cell is $\bar{\bar{\rho}} = \frac{1}{4} \times (\bar{\rho}_1 + \bar{\rho}_2 + \bar{\rho}_3 + \bar{\rho}_4)$.

The corresponding AGPE integrated over the area of the first sub-cell is

$$\prod_{A_i}^{a} = -\frac{g}{2}\int dz \int_{-1/2}^{1/2} dy \int_{-1/2}^{1/2} \frac{(\rho_{x,1}x + \rho_{y,1}y + \rho_{\Delta,1}xy + \bar{\rho}_1 - \bar{\bar{\rho}})^2}{\bar{\rho}_z^{\theta}} dx,$$

where the reference state $\bar{\bar{\rho}}$ is defined by horizontal averaging of the density field in the four sub-cells, and $\bar{\bar{\rho}}_z^{\theta}$ is the vertical gradient of the potential density averaged over the four sub-cells. Integrating over each sub-cell and summing up, the total AGPE in each $2° \times 2°$ grid cell is

$$\prod_{i,j}^{a} = -\frac{g}{2}\sum_{k=1}^{km}\sum_{i=1}^{4}\left[\frac{1}{12}\left(\rho_{x,i}^2 + \rho_{y,i}^2 + \frac{1}{12}\rho_{\Delta,i}^2\right) + (\bar{\rho}_i - \bar{\bar{\rho}})^2\right](\bar{\bar{\rho}}_z^{\theta})^{-1} A_i \Delta Z_k,$$

where km is the lowest level of the water column in this grid cell, and A_i is the area of each sub-cell.

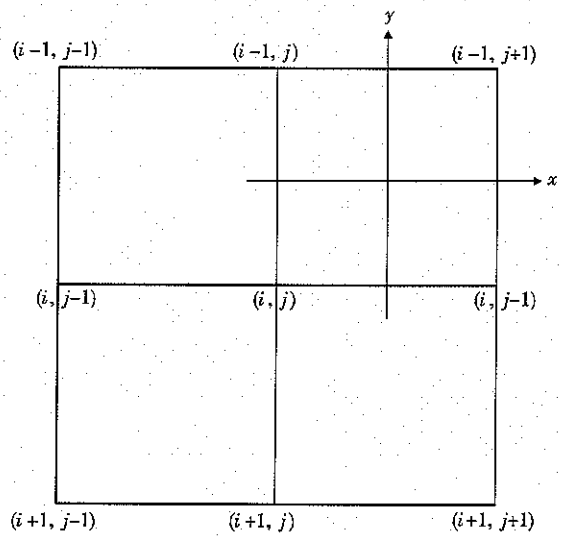

Fig. A1. Sketch of a nine-point $2° \times 2°$ grid cell in a resolution.